Mechanics of light-activated self-healing polymer networks

Kunhao Yu, An Xin, Qiming Wang*

Sonny Astani Department of Civil and Environmental Engineering, University of Southern California, Los Angeles, CA 90089, USA

A B S T R A C T

Optically healable polymers represent an interesting stimuli-responsive self-healing material as the healing process can be controlled on-demand and remotely. The fundamental mechanism of the light-activated interfacial self-healing process has not been theoretically understood. Here, we present a theoretical framework to understand the light-activated interfacial self-healing of soft polymers with light-responsive photophores. We consider that the light propagation through the material matrix triggers the production of free radicals that facilitate the interfacial self-healing process. The self-healing process is considered as a coupled behavior that polymer chains diffuse across the interface and re-form the dynamic bonds assisted by the free radicals. We theoretically relate the light property to the interfacial self-healing strength of the polymers. We predict that the interfacial self-healing strength of the polymer increases with the light illumination time until reaching a plateau. We theoretically explain the effects of the light intensity, light wavelength, and photoinitiator concentration on the self-healing performance. We then apply the theory to two types of soft polymers with inorganic and organic photophores, respectively. The experimentally measured stress–strain behaviors of the original and self-healed samples can be consistently explained by the theory. The experimentally measured relationships between the healing strength and the healing time also agree well with the theoretical results.

© 2018 Elsevier Ltd. All rights reserved.

1. Introduction

The self-healing polymers capable of self-repairing fractures or damages have shown great potential in a number of applications, such as flexible electronics (Tee et al., 2012), energy storage (Wang et al., 2013b), biomaterials (Brochu et al., 2011), and robotics (Terryn et al., 2017). These self-healing polymers, either relying on encapsulates of curing agents (Blaiszik et al., 2010; Cho et al., 2006; Keller et al., 2007; Toohey et al., 2007; White et al., 2001), or various dynamic bonds (Bhattacharya and Samanta, 2016; Burnworth et al., 2011a; Chen et al., 2002, 2012; Cordier et al., 2008; Ghosh and Urban, 2009; Haraguchi et al., 2011; Holten-Andersen et al., 2011; Hu and Chen, 2014; Liu et al., 2015; Mayumi et al., 2016; Nakahata et al., 2011; Phadke et al., 2012; Rose et al., 2013; Satarkar et al., 2010; Sijbesma et al., 1997; Skene and Lehn, 2004; Sun et al., 2012, 2013; Wang et al., 2013a, 2013b, 2017, 2010; Yu et al., 2018b), can usually activate the interfacial bridging mechanism under an adequate condition when the fractured interfaces are brought into contact. Among these self-healing polymers, the ones with self-healing behaviors responsive to the remote stimuli are especially interesting; because the remote stimuli can usually be delivered locally to achieve on-demand self-healing performance.

Optically healable polymer is a type of stimuli-responsive self-healing polymer that harnesses the external visible or ultraviolet (UV) light to activate the self-healing reaction around the fracture interface (Amamoto et al., 2011, 2012; Balkenende et al., 2016; Burnworth et al., 2011b; Fiore et al., 2013; Froimowicz et al., 2011; Habault et al., 2013; Ji et al., 2015; Ling et al., 2012; Liu et al., 2013; Michal et al., 2013; Otsuka et al., 2010; Yu et al., 2018a; Zhang and Zhao, 2013). Within

---

* Corresponding author.
  E-mail address: qimingw@usc.edu (Q. Wang).
https://doi.org/10.1016/j.jmps.2018.11.019

the optically self-healable polymers, a special photo-responsive chemical group called "*photophore*" is incorporated within the polymer network. When two fractured interfaces are brought into contact under the exposure of light with an adequate wavelength, the light-triggered free radicals will activate the photophore to facilitate the polymer-chain rebinding to bridge the fractured interface. The photophores can usually be divided into two types: organic photophores and inorganic photophores. The organic photophores include special photo-responsive organic chemical groups (Amamoto et al., 2011, 2012; Balkenende et al., 2016; Froimowicz et al., 2011; Ji et al., 2015; Ling et al., 2012; Michal et al., 2013; Otsuka et al., 2010). The inorganic photophores include metal-organic frameworks (Burnworth et al., 2011b) and nanoparticles or nanosheets (Liu et al., 2013; Yu et al., 2018a). These optically healable polymers with diverse photophores provide a representative paradigm of stimuli-controlled self-healing and offer great potential for a wide range of on-demand healing applications (Fiore et al., 2013; Habault et al., 2013).

Despite the great potential, the theoretical modeling of the underlining self-healing mechanism of the light-activated self-healing is not available. Though mechanics models for the constitutive behaviors of light-activated polymers have been proposed (Long et al., 2011, 2009, 2013; Ma et al., 2014), how to model the light-activated interfacial self-healing behavior remains elusive. For example, how the light activates the photophores during the self-healing process remains unknown. How the light-triggered free radicals activate the polymer chain evolution around the healing interface remains unclear. And how the light properties including intensity and wavelength affect the self-healing performance is also ambiguous. If theoretical models for the light-activated interfacial self-healing are successfully established, the future design and optimization of these materials will be significantly facilitated. The theory may also be extended to model the self-healing behaviors of polymers under various other stimuli, such as heat, pH value, and electromagnetic fields (Blaiszik et al., 2010; Burattini et al., 2010; Roy et al., 2015; Thakur and Kessler, 2015; Wool, 2008; Wu et al., 2008).

Here, we establish a theoretical framework to model the light-activated interfacial self-healing of light-responsive polymer networks. We consider that light-triggered free radicals around the healing interface can facilitate the interpenetration of the polymer chain to bridge the fracture interface. We consider two groups of coupled diffusion-reaction systems around the healing interface: one for the light-activated production of free radicals, and the other for the polymer chain diffusion and distal-group binding kinetics. We apply the theoretical framework to two types of soft polymers with inorganic nanoparticle photophores and organic photophores, respectively. We predict that the healed interfacial strengths for both polymers increase with light-illumination-associated healing time until reaching plateaus. We also elucidate the effects of the light intensity, the light wavelength, and the photoinitiator concentration on the self-healing performance. The theoretical calculations can consistently agree with the experimental results of light-activated self-healing of soft polymers with inorganic and organic photophores, respectively.

The plan of this paper is as follows: In Section 2, we introduce the experimental procedure and results of optically healable TiO₂ nanocomposite hydrogels. In Section 3, we construct the theoretical frameworks of light-activated production of free radicals and radical-assisted polymer-chain interpenetration across the healing interface. We then apply the theories to soft polymers with inorganic nanoparticle photophores and organic photophores, respectively. Subsequently, in Sections 4 and 5, we present the theoretical results of light-activated self-healing of soft polymers with respective inorganic and organic photophores. The theoretical results are compared with the corresponding experimental measurements. The conclusive remarks are presented in Section 6.

2. Experiments of hydrogels with inorganic photophores TiO₂ nanoparticles

We will study the light-activated self-healable polymer networks with nanoparticle and organic photophores. The experiments of light-activated self-healable polymer networks with organic photophores are shown in (Amamoto et al., 2012). We introduce the experiments of light-activated self-healable polymer networks with representative TiO₂ particle photophores in this section. We hope the study can be extended to explain other light-activated self-healable polymer networks with various particle photophores.

TiO₂ nanoparticles dispersion (Anatase, 15 wt%, 5–15 nm, crosslinker) was purchased from US Research Nanomaterials. Acrylamide (AAm, monomer), N,N-Dimethylacrylamide (DMAA, monomer), potassium peroxodisulfate (KPS, photoinitiator), and N,N,N′,N′-Tetramethylethylenediamine (TEMED, accelerator) were purchased from Sigma-Aldrich (United States). All chemicals were used as received without further purification. The 10 g TiO₂ solution was first bubbled with nitrogen for 30 min to remove the oxygen dissolved in the solution. Then, the solution was mixed with 0.039 g (0.009 mol) AAm and 2.079 g (0.021 mol) DMAA under the magnetic stirring for 30 min at 20 °C. The mixed solution was cooled down to 0 °C in an iced water bath. 0.1 wt% KPS and 8 μL TEMED were then added in with another 30 min stirring. The obtained solution was poured into a glass tube (diameter 11 mm and length 50 mm) or a glass mold (150 mm × 75 mm × 3 mm) with the cover up to avoid contact with the oxygen. To facilitate the in-situ free-radical polymerization, the hydrogel was put in a UV chamber (UVP CL-1000 Ultraviolet Crosslinker) with light intensity 37 W/m² (Five 8 Watt light bulbs with 254 nm wave length) for 30 min (Fig. 1a). Note that The TiO₂ nanoparticles and the polymer chains are bonded through dynamic bonds, such as hydrogen bonds (between -OH on the particle surface and -NH₂ group on polymer chains) (Liu et al., 2013; Xu et al., 2013), or ionic bonds (between K⁺ groups from redox initiator KPS and anionic groups of the polymer chains) (Haraguchi, 2007, 2011; Haraguchi and Takehisa, 2002; Thakur and Kessler, 2015).

For the characterization of the self-healing behavior, cylindrical hydrogel samples (diameter 11 mm, length 10 mm) were cut into two pieces with a blade and then were brought into contact with the additional force for 30 s on two sides to
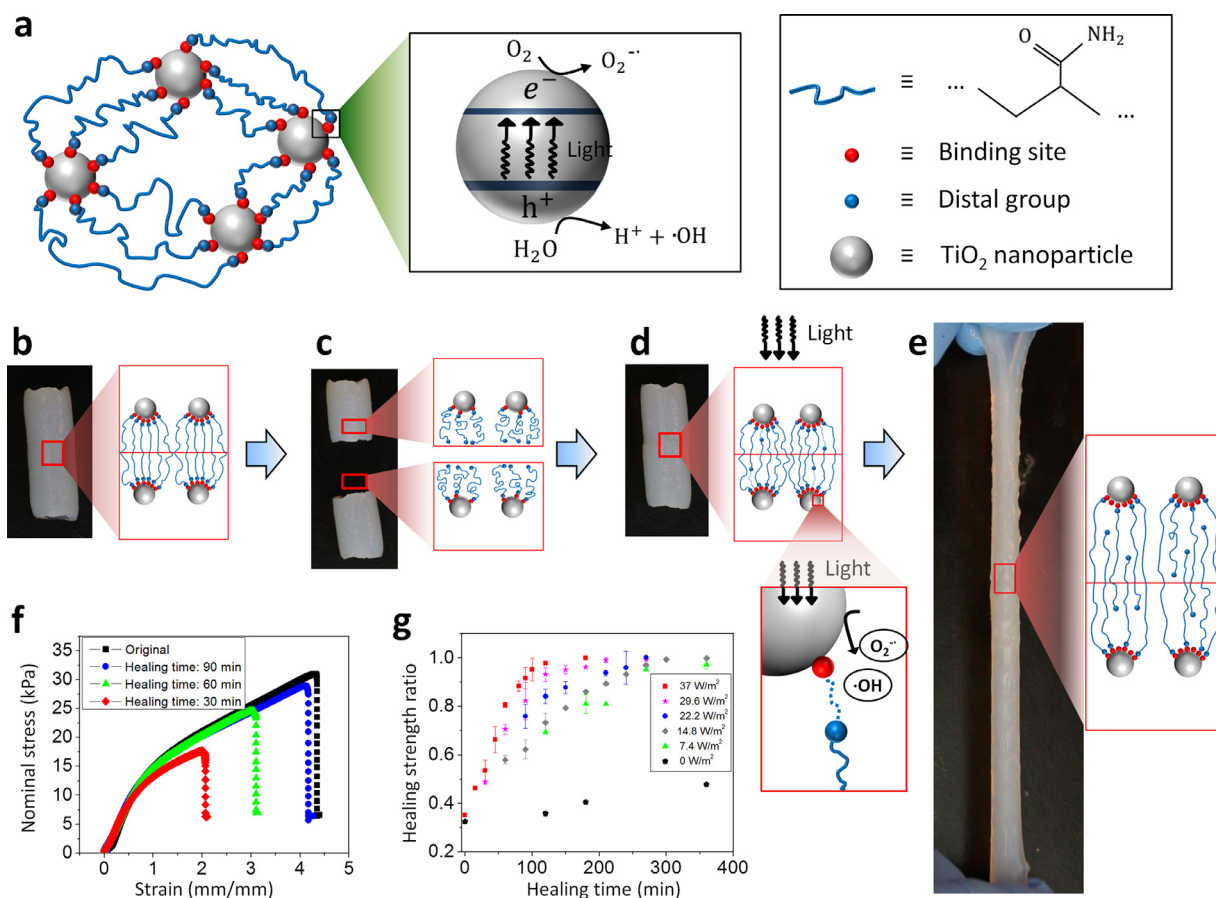
Fig. 1. (a) A schematic to show the polymer chain network of the TiO_2 nanocomposite hydrogel and the related light-triggered production of free radicals. (b–e) A typical self-healing experiment of TiO_2 nanocomposite hydrogel. A hydrogel sample is first cut into two parts and then immediately brought into contact with the UV illumination. After a period of healing time, the sample can be stretched again. (f) Nominal stress–strain behaviors for the original and healed hydrogel samples. (g) Healing strength ratio of self-healed samples as functions of healing time for various UV intensities. The healing strength ratio is calculated as the nominal strength of the self-healed sample normalized by the nominal strength of the original sample.

ensure the cut surfaces have good enough contact during the healing process (Fig. 1b–d). The samples were then put into UV chamber with different light intensities (7.4 W/m², 22.2 W/m² and 37 W/m²) and controlled moisture using wet paper to avoid the swelling and de-swelling behavior of the samples. The self-healed samples were then stretched uniaxially until ruptures using the same testing system (Instron, Model 5942) with strain rate 0.06 s^{-1} at 20°C (Fig. 1e). We found that the original hydrogel ruptured at a strain around 4.3 (Fig. 1f). The corresponding nominal stress was denoted as the uniaxial strength. As the healing time increased, the uniaxial strength increased until a plateau of the original uniaxial strength (Fig. 1g). However, the uniaxial strength of the contacted samples without the illumination of the UV light only showed a slight increase, and could not reach the original strength even when the healing time is 6–7 h. Besides, we found that the healing process of the TiO_2 nanocomposite hydrogels becomes more rapid as the UV light intensity increases (Fig. 1g).

3. Theoretical model

3.1. A general theory for light-activated interfacial healing

With the presence of photoinitiators in the polymer matrix, the light can trigger the production of free radicals (Fig. 2). The basic process is shown in Fig. 2. The free radicals will assist the binding of the open distal groups on a polymer chain to become an active binding site (RM• shown in Fig. 2), thus to bridge the fractured interface. In soft polymers with nanomaterial photophores, the active binding site is on the nanomaterial surface. In soft polymers with organic photophore, the active binding site is the open distal group on a polymer chain within the counterpart matrix. In Section 3.1.1, we will model the light-activated production of free radicals; and in Section 3.1.2, we will then model the radical-assisted chain rebinding. In the subsequent Sections 3.2 and 3.3, we will apply the general model for light-activated interfacial healing to soft polymers with nanomaterial photophores and organic photophores, respectively.
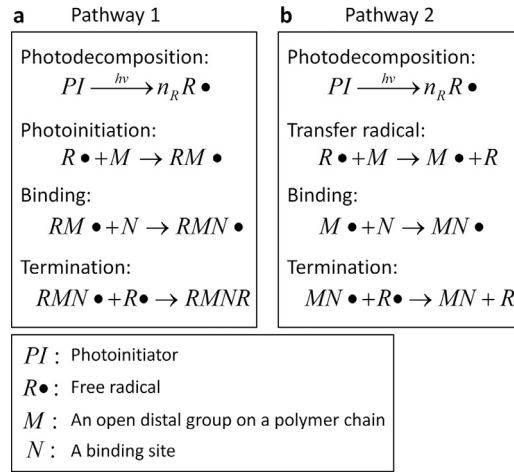
Fig. 2. Two possible pathways for the photoinitiated binding process between an open distal group on a polymer chain and a binding site. (a) Pathway 1: The photoinitiator (PI) is first decomposed into n_R free radicals (R•). A radical binds with the open distal group to form a distal radical (RM•). The distal radical reacts with the binding site and then is terminated by another radical. (b) Pathway 2: The photoinitiator (PI) is first decomposed into n_R free radicals (R•). A radical transfers to the open distal group to form a distal radical (M•). The distal radical reacts with the binding site and then is terminated by another radical.
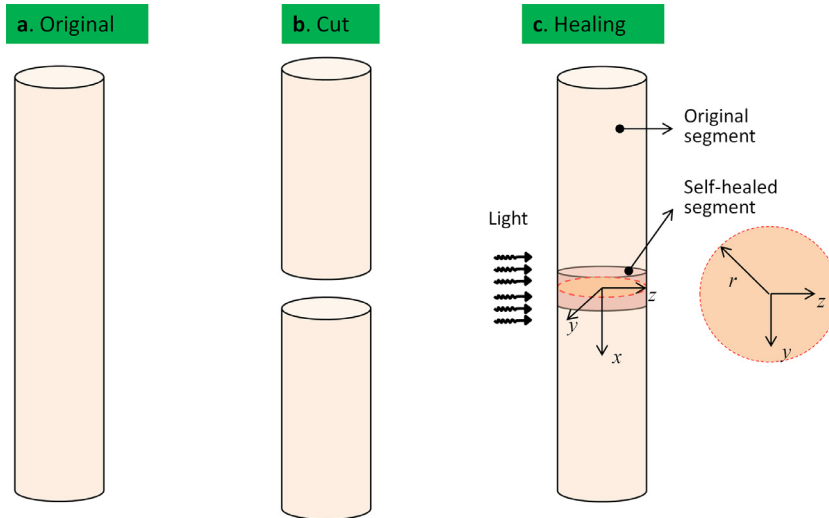

Fig. 3. Schematics to show the experimental procedure. The global Cartesian coordinate system is constructed on the healing interface. The light illumination direction is along the z-axis.

3.1.1. Light-activated production of free radicals

When light with an initial light intensity I_0 is illuminated on a polymer material, the light will be attenuated through the material matrix. The light propagation can be modeled by the Beer–Lambert law (Long et al., 2011, 2009, 2013),

$$\frac{\partial I(\mathbf{x}, t)}{\partial z} = -A(\mathbf{x}, t) I(\mathbf{x}, t) \tag{1}$$

where $I(\mathbf{x}, t)$ is the light intensity at position $\mathbf{x} = (x, y, z)^T$ and time t, the light propagation direction is along the z-axis (Fig. 3), and $A(\mathbf{x}, t)$ is the absorption coefficient of the material. The light-sensitive polymers contain photoinitiators that absorb light to produce free radicals (Fig. 2). Within the nanocomposite polymers, nanomaterials such as TiO_2 usually serve as the photoinitiator; while in other light-sensitive polymers, organic photoinitiators are employed. In both cases, the absorption coefficient can be estimated as

$$A(\mathbf{x}, t) \approx \alpha_1 C_I(\mathbf{x}, t) + A_{mat} \tag{2}$$

where $C_I(\mathbf{x}, t)$ is the concentration of the photoinitiator, α_1 is the molar absorptivity of the photoinitiator, and A_{mat} is the absorption coefficient of the material matrix. For the nanocomposite polymers, $C_I(\mathbf{x}, t)$ is the concentration of the photosensitive nanomaterial such as TiO_2 nanoparticles.
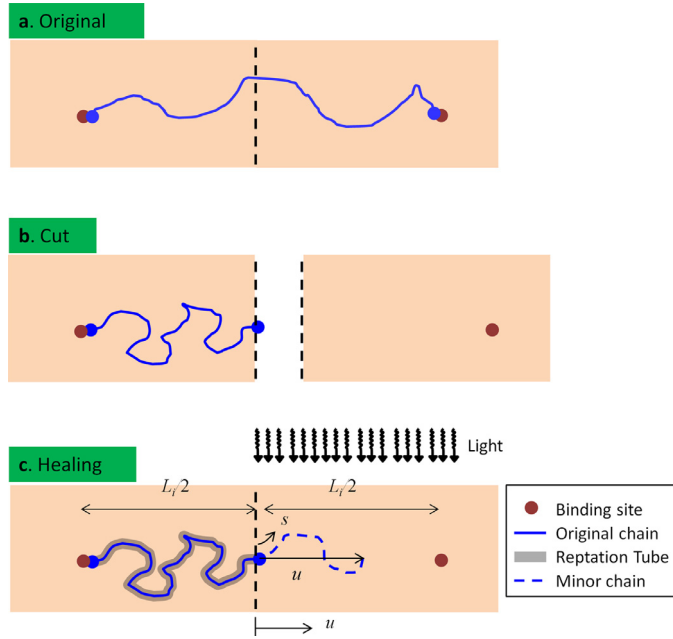
Fig. 4. Schematics to show the polymer chain behaviors around the healing interface. (a) At the original state, a polymer chain is bond by two binding sites across the cutting interface. (b) The cutting forces the detachment between the polymer chain and one binding site. Since we immediately contact two fractured parts, we assume the distal group of the polymer chain is still around the interface. (c) During the healing process, the distal group migrates into the counterpart to find and bind the binding site under the activation of the UV light.

With the local light intensity $I(\mathbf{x}, t)$, free radicals are produced from the photoinitiator. The governing equation of the concentration of the free radical $C_R(\mathbf{x}, t)$ can be written as (Long et al., 2011, 2009, 2013; Ma et al., 2014; Wu et al., 2018; Zhao et al., 2015, 2016)

$$\frac{\partial C_R(\mathbf{x}, t)}{\partial t} = n_R \alpha_2 C_I(\mathbf{x}, t) I(\mathbf{x}, t) + D_R \nabla^2 C_R(\mathbf{x}, t) - k_t [C_R(\mathbf{x}, t)]^2 \tag{3}$$

where α_2 is the light absorption coefficient for the radical production, n_R is the number of radicals produced per photoinitiator, D_R is the diffusivity of the radical, k_t is the termination rate of the radical. Here, we assume the combination of two radicals will result in a termination of the radicals; therefore, the termination term involves a square term $[C_R(\mathbf{x}, t)]^2$. Note that for the organic photoinitiator, one photoinitiator is usually decomposed into two radicals, and thus $n_R = 2$ (Fig. 2). However, for a nanomaterial photoinitiator such as TiO_2, n_R is an unknown large number that varies for nanoparticles with different activities (Bueche, 1960; Wang and Gao, 2016).

Along with the production of radicals, the photoinitiator concentration of the nanocomposite may not change, i.e., $C_I(\mathbf{x}, t) = \eta$, where η is the nanomaterial volume concentration. However, the concentration of the organic photoinitiator may change with a governing equation written as (Long et al., 2011, 2009, 2013)

$$\frac{\partial C_I(\mathbf{x}, t)}{\partial t} = -\alpha_2 C_I(\mathbf{x}, t) I(\mathbf{x}, t) + D_I \nabla^2 C_I(\mathbf{x}, t) \tag{4}$$

where D_I is the diffusivity of the organic photoinitiator. Given an initial light intensity and material geometry Fig. 3), we can calculate the concentration distribution of the radical within the material matrix from Eqs. (1–4). The theoretical results are presented in Sections 4.1 and 4.2.

3.1.2. Radical-assisted chain binding

The sample is first cut into two parts, and then immediately brought into contact to heal the interface with the illumination of a UV light (Fig. 4). During the cutting process, the dynamic bonds that crosslink the polymer chains will be dissociated by the large force induced by the cutting (Fig. 4a and b). We assume one distal group of the chain is dissociated from a binding site that is within the matrix, and then this distal group will be pulled out of the matrix to the fracture interface. Since the healing experiment is carried out immediately after the cutting, we assume the open distal group on the chain will still be around the interface at the very beginning of the healing process (Fig. 4b and c), primarily because the migration of the chain and its distal group takes substantial time. During the healing process, the polymer chain with the open distal group will gradually diffuse cross the interface to find the binding site to reform the dynamic bond. Once the dynamic bond is reformed (or re-associated), the polymer chain becomes linked and can sustain loading forces.

We assume the original polymer networks crosslinked by the dynamic bonds consist of m types of chains with Kuhn segment number n_1, n_2, ... and n_m, respectively. Each Kuhn segment has a length b. The specific polymer network architecture will be discussed in Sections 3.2 and 3.3. Here, we only focus on the ith chain with Kuhn segment number n_i, where $1 \le i \le m$. The number of ith chain per unit volume of material is N_i.

The re-binding process of the ith chain involves the chain diffusion and distal group reaction. We first model the binding between the open distal group and the binding site as a chemical reaction. This chemical reaction involves multiple small processes shown as two representative pathways in Fig. 2a,b. In the first pathway (Fig. 2a), the free radical binds on the open distal group on the ith chain to become a distal radial. Then, the distal radical binds on the binding site. Finally, the radical will be terminated by combining with another free radical. Effectively, the reaction involves two radicals, an open distal group on the ith chain, and a binding site. In the second pathway (Fig. 2b), the photoinitiator (PI) is first decomposed into n_R free radicals (R•). A radical transfers to the open distal group to form a distal radical (M•). The distal radical reacts with the binding site and then is terminated by another radical.

This re-binding process turns an open ith chain into a linked ith chain. We denote $C_i^d(s, t)$ as the open ith chain number per unit length along the curvilinear coordinate s ($0 \le s \le L_i^2/4b$) at time t (Fig. 4c), and $C_i^a(s, t)$ as the corresponding linked quantity. We further denote the reaction from the open chain to the linked chain as the forward reaction and the else as the reverse reaction. The reaction kinetics can be written as

$$\frac{\partial C_i^a(s, t)}{\partial t} = k_i^{f0} C_i^d(s, t) - k_i^{r0} C_i^a(s, t) \tag{5}$$

where k_i^{f0} is the forward reaction rate and k_i^{r0} is the reverse reaction rate. We further assume that the self-healing capability of the studied polymer is relatively strong; that is to say, the association reaction rate k_i^{f0} is much larger than the dissociation reaction rate k_i^{r0}. Therefore, Eq. (5) can be reduced to

$$\frac{\partial C_i^a(s, t)}{\partial t} \approx k_i^{f0} C_i^d(s, t) \tag{6}$$

As shown in Fig. 2a and b, the presence of free radicals significantly facilitates the re-association process of the ith chain. The forward reaction rate can be approximated as

$$k_i^{f0} = k_1 [C_R(\mathbf{x}, t)]^2 \tag{7}$$

where k_1 is a positive coefficient and the square term is because of the presence of two radicals per reaction (Fig. 2a and b).

The radical-assisted binding will facilitate the chain diffusion to cross the healing interface. The chain diffusion can be modeled by following a snake reptation model proposed by De Gennes (De Gennes, 1979, 1971; Doi and Edwards, 1978; Rubinstein and Colby, 2003). The basic idea is that the polymer chain is constrained by the polymer matrix so it can only reptate along a primitive tube (Doi and Edwards, 1988). The primitive tube length is L_c, so the original chain is divided into n_i segment with each segment length

$$b_c = \frac{L_c}{n_i} \tag{8}$$

At each small time step, the chain is considered to jump by a step length b_c in a random-walk fashion. In the original reptation model, the tube length is considered as smaller than the contour length of the ith chain, i.e., $L_c \le n_i b$; because the chain may coil around the reptation tube. Subsequently, the jump step b_c is considered as an unknown parameter. Here, we make a bold assumption that the contour length of the ith chain is approximately equal to the reptation tube length; therefore, the jump step length

$$b_c \approx b \tag{9}$$

The motion of the polymer chain is enabled by extending out small segments called "minor chains" (Fig. 4c). The curvilinear motion of the polymer chain is characterized by the Rouse friction model with the curvilinear diffusivity of the ith chain expressed as

$$D_i = \frac{k_B T}{n_i \xi} \tag{10}$$

where ξ is the Rose friction coefficient per unit Kuhn segment, k_B is the Boltzmann constant, and T is the temperature in Kelvin.

As shown in Fig. 4c, we assume the end-to-end distance of the ith chain is L_i. Without loss of generality, we assume the cutting position is located in the middle of the chain; thus, the distance between the healing interface and the binding site is $L_i/2$. This assumption is just for the sake of analysis simplicity; other location may also work but may involve more complicated statistic averaging algorithm. As shown in Fig. 4c, the distal group will diffuse cross the normal distance $L_i/2$ following a curvilinear pathway. To facilitate the analysis, we construct two coordinate systems: s denotes the curvilinear path along the minor chains, and u denotes the linear path from the interface to the binding site. When the ith chain

moves s_i distance along the curvilinear path, it is corresponding to u_i distance along u coordinate. Here we assume the selection of the curvilinear path is stochastic in a random-walk fashion (Kim and Wool, 1983; Whitlow and Wool, 1991; Zhang and Wool, 1989). Therefore, the conversion of the distances in two coordinate systems is expressed as (de Gennes, 1971; Doi and Edwards, 1988)

$$u_i = \sqrt{s_i b_c} \approx \sqrt{s_i b} \tag{11}$$

According to Eq. (11), the $L_i/2$ in the y coordinate is corresponding to $L_i^2/4b$ in the s coordinate.

The chain diffusion and the association reaction are strongly coupled, as the binding reaction may greatly facilitate the diffusion process; therefore, we couple the chain diffusion and binding reaction within the region $0 \leq s \leq L_i^2/4b$ using an effective diffusion-reaction equation as

$$\frac{\partial C_i^d(s,t)}{\partial t} = D_i \frac{\partial^2 C_i^d(s,t)}{\partial s^2} - \frac{\partial C_i^a}{\partial t} \tag{12}$$

Coupled with Eqs. (6), (7) and (12) can be rewritten as

$$\frac{\partial C_i^d(s,t)}{\partial t} = D_i \frac{\partial^2 C_i^d(s,t)}{\partial s^2} - k_1[C_R(\mathbf{x},t)]^2 C_i^d(s,t) \tag{13}$$

It can be shown from Eq. (13) that the light-triggered production of radicals can facilitate the binding reaction and thus promote the chain diffusion.

At the beginning of the healing process, all mobile open distal groups of the ith chain are located around the healing interface, which can be expressed as

$$C_i^d(s, t=0) = N_i \delta(s) \tag{14}$$

$$C_i^a(s, t=0) = 0 \tag{15}$$

where $\int_{-\infty}^{\infty} \delta(s) = 1$. Besides, we assume the association reaction rate is much larger than the dissociated reaction rate; subsequently, we can make a bold assumption that all open distal groups form dynamic bonds around the binding site location $s = L_i^2/4b$, which is expressed as

$$C_i^d\left(s = L_i^2/4b, t\right) \approx 0 \tag{16}$$

From Eqs. (13–16), we can solve the concentration distributions $C_i^d(s,t)$ within the curvilinear coordinate. To convert these to the effective concentration of linked ith chain within the region $0 \leq u \leq L_i/2$, we write

$$\frac{N_i^h(t)}{N_i} = 1 - \frac{4b}{L_i^2} \int_0^{L_i^2/4b} \frac{C_i^d(s,t)}{N_i} ds \tag{17}$$

where $N_i^h(t)$ is the average ith chain number per unit volume of the region $0 \leq u \leq L_i/2$ at the undeformed state ($\lambda_1 = \lambda_2 = \lambda_3 = 1$), and the superscript "$h$" denotes "healed".

3.2. Model for soft polymers with nanomaterial photophores

In this section, we apply the general theory of the light-activated interfacial self-healing to soft polymers with nanomaterial photophores such as TiO$_2$ nanoparticles (Yu et al., 2018a). The nanomaterials serve as multifunctional crosslinkers that are able to bridge a large number of polymer chains (Figs. 1 and 5a and b). These polymer chains may not have the same chain length, but follow an inhomogeneous chain length distribution (Fig. 5c). Following our previous paper on nanocomposite hydrogels, we assume the nanomaterial crosslinkers self-organize into body-centered cubes through the whole material matrix (Fig. 5a). Like the eight-chain model, the center nanocrosslinker and a corner nanocrosslinker bridge m types of chains with chain lengths number n_1, n_2, ... and n_m. The distance between the center nanocrosslinker and the corner nanocrosslinker L_i can be estimated from the volume concentration of the nanocrosslinker η. A cube in Fig. 5a with a volume $8L_i^3/3\sqrt{3}$ averagely involve two nanocrosslinkers; therefore,

$$L_i \approx \frac{\sqrt{3}}{\sqrt[3]{4\eta}} \tag{18}$$

We denote the ith chain number between a center nanocrosslinker and a corner nanocrosslinker as N_i^*. As we assume the chain number of the ith chain per unit volume as N_i, we have

$$N_i = \frac{8N_i^*}{\frac{8}{3\sqrt{3}}L_i^3} = \frac{3\sqrt{3}N_i^*}{L_i^3} \tag{19}$$
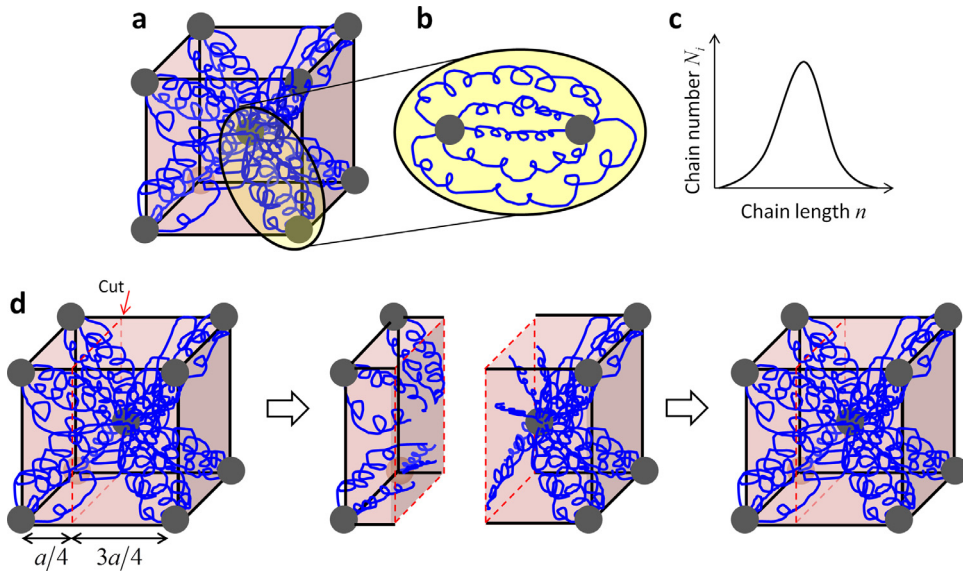
Fig. 5. (a) A network model for the nanocomposite hydrogel. (b) A number of polymer chains with inhomogeneous chain lengths are bridged between a particle pair. (c) A schematic to show the chain-length distribution of the polymer chains between a particle pair. (d) Schematics of the network model during the cutting and healing process. The cutting is assumed to be located in a quarter position of the cube.

We thus calculate N_i^* as

$$N_i^* = \frac{N_i}{4\eta} \tag{20}$$

The chain length distribution of these m types of chains can be written as

$$P_i(n_i) = \frac{N_i}{\sum_{i=1}^{m} N_i} \tag{21}$$

For simplicity, we only consider a log-normal chain length distribution as (Wang et al., 2015)

$$P_i(n_i) = \frac{1}{n_i \delta \sqrt{2\pi}} exp\left[-\frac{(\ln n_i - \ln n_a)^2}{2\delta^2} \right] \tag{22}$$

where n_a and δ are the mean of n_i and standard deviation of $\ln n_i$, respectively.

For the ith chain, the freely-joint end-to-end distance is $\sqrt{n_i}b$. The presence of nanocrosslinker makes the initial end-to-end distance as L_i. As the ith chain is deformed with the end-to-end distance r_i, the chain stretch is calculated as

$$\Lambda_i = \frac{r_i}{\sqrt{n_i}b} \tag{23}$$

The free energy of the deformed ith chain can be written as

$$w_i = n_i k_B T \left(\frac{\beta_i}{\tanh \beta_i} + \ln \frac{\beta_i}{\sinh \beta_i} \right) \tag{24}$$

where $\beta_i = L^{-1}(\Lambda_i/\sqrt{n_i})$ and $L^{-1}()$ is the inverse Langevin function. The force within the deformed ith chain can be written as

$$f_i = \frac{\partial w_i}{\partial r_i} = \frac{k_B T}{b} \beta_i \tag{25}$$

We consider an affined deformation model with the assumption that the bond-centered cube deforms by three principal stretches ($\lambda_1, \lambda_2, \lambda_3$) under the macroscopic deformation ($\lambda_1, \lambda_2, \lambda_3$) at the material level. Therefore, the stretch of each ith chain is

$$\Lambda_i = \sqrt{\frac{\lambda_1^2 + \lambda_2^2 + \lambda_3^2}{3}} \frac{L_i}{\sqrt{n_i}b} \tag{26}$$

For the original material, the initial number of ith chain per unit material volume is N_i. This ith chain density will decrease to N_i^a as the material deforms because the chain force will motivate the dissociation of the dynamic bond between

the chain the nanocrosslinker. Following Eq. (5), we write the binding reaction kinetics as

$$\frac{dN_i^a}{dt} = k_i^f N_i^d + k_i^r N_i^a \tag{27}$$

where k_i^f and k_i^r are forward and reverse reaction rates at the deformed state, respectively. Following the Bell's model (Bell, 1978), we can write the chain-force-dependent reaction rates as

$$k_i^f = k_i^{f0} \exp\left(-\frac{f_i \Delta x}{k_B T}\right) \tag{28a}$$

$$k_i^r = k_i^{r0} \exp\left(\frac{f_i \Delta x}{k_B T}\right) \tag{28b}$$

where Δx is the distance along the energy landscape coordinate. If the loading is applied quasistatically, the linked ith chain volume density can be calculated as

$$N_i^a = \frac{N_i k_i^{f0} \exp\left(-\frac{f_i \Delta x}{k_B T}\right)}{k_i^{r0} \exp\left(\frac{f_i \Delta x}{k_B T}\right) + k_i^{f0} \exp\left(-\frac{f_i \Delta x}{k_B T}\right)} \tag{29}$$

As shown in Eq. (29), N_i^a decreases as the chain force of the ith chain increases.

With Eqs. (24) and (29), we can express the strain energy per unit material volume as

$$W = \sum_{i=1}^m N_i^a n_i k_B T \left(\frac{\beta_i}{\tanh \beta_i} + \ln \frac{\beta_i}{\sinh \beta_i}\right) \tag{30}$$

where $\beta_i = L^{-1}(\Lambda_i/\sqrt{n_i})$ and Λ_i is given in Eq. (26). If the material is incompressible and uniaxially stretched with three principal stretches ($\lambda_1 = \lambda, \lambda_2 = \lambda_3 = \lambda^{-1/2}$), the nominal stress along λ_1 direction can be written as

$$s_1 = \frac{(\lambda - \lambda^{-2})k_B T}{\sqrt{3\lambda^2 + 6\lambda^{-1}}} \sum_{i=1}^m \left[N_i^a \frac{L_i}{b} L^{-1}\left(\sqrt{\frac{\lambda^2 + 2\lambda^{-1}}{3}} \frac{L_i}{n_i b}\right)\right] \tag{31}$$

As the stretch increases, the chain forces on the short chains are larger than those on the long chains; the short chains will be first detached from the nanoparticles and then the long chains (Fig. 5c). When the stretch is sufficiently large, the majority of chains are detached from the nanoparticles, and the corresponding stress would decrease with the increasing stretch. Therefore, the stress-stretch behavior of the original material features a maximal stress that is defined as the tensile strength of the material.

In the healing experiment, we first use a sharp blade to cut through the hydrogel bar (Figs. 3 and 5d). For simplicity of analysis, we assume the cutting position is located in the middle of polymer chains between particle pairs as shown in Fig. 5d (Wang et al., 2017; Yu et al., 2018b). This echoes the assumption in Section 3.1.2 that the cutting location is in the middle of two binding sites shown in Fig. 4b. At the cutting tip, the blade highly deforms the polymer chains until the chains are detached from the particles. Since the chain strength is much larger than the chain-particle bonding strength, we assume that the polymer chains can only be detached from the particle surfaces without breaking in the middle of the chains (Wang and Gao, 2016). At the detachment point, the chain may be detached from either particle, with the other end being still attached to the other particle. We assume that each particle of a particle-pair still attach half portion of polymer chains after cutting (Fig. 5d). Then two parts are immediately brought into contact with the polymer chains interpenetrate into each other to rebind on the particles.

For the self-healing sample that is composed of two original segments and a small self-healed segment (Fig. 3c). Within the self-healed segment, the strain energy per unit material volume is

$$W = \sum_{i=1}^m N_i^{ah} n_i k_B T \left(\frac{\beta_i}{\tanh \beta_i} + \ln \frac{\beta_i}{\sinh \beta_i}\right) \tag{32}$$

$$N_i^{ah} = \frac{N_i^h k_i^{f0} \exp\left(-\frac{f_i \Delta x}{k_B T}\right)}{k_i^{r0} \exp\left(\frac{f_i \Delta x}{k_B T}\right) + k_i^{f0} \exp\left(-\frac{f_i \Delta x}{k_B T}\right)} \tag{33}$$

where N_i^h is given by Eq. (17). If the material is uniaxially stretched by λ^h, the corresponding nominal stress is

$$s_1^h = \frac{(\lambda^h - \lambda^{h-2})k_B T}{\sqrt{3\lambda^{h2} + 6\lambda^{h-1}}} \sum_{i=1}^m \left[N_i^{ah} \frac{L_i}{b} L^{-1}\left(\sqrt{\frac{\lambda^{h2} + 2\lambda^{h-1}}{3}} \frac{L_i}{n_i b}\right)\right] \tag{34}$$

If the self-healed sample is uniaxially stretched (like Fig. 1e), the nominal stresses in the original material segment and the self-healed segment should be equal, i.e., $s_1^h = s_1$. Based on the above theoretical framework, we can calculate the stress–strain behaviors of the self-healed sample and the corresponding healing strength for various healing time (results in Section 4).
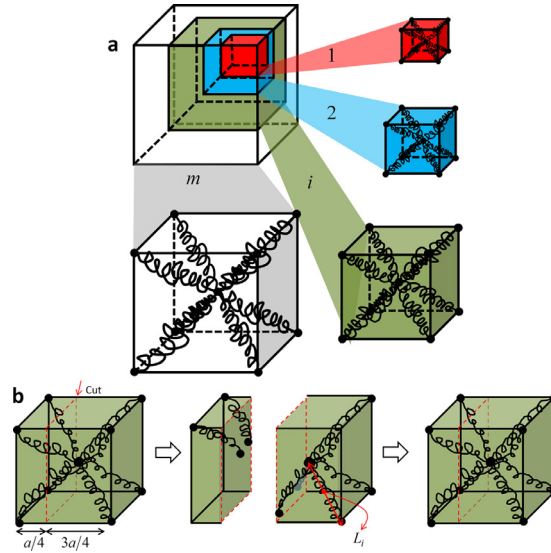
Fig. 6. (a) An interpenetration network model for the light-activated self-healing polymers with organic lightophores. (b) Schematics of the *i*th network model during the cutting and healing process. The cutting is assumed to be located in a quarter position of the cube.

3.3. Model for soft polymers with organic photophores

In this section, we apply the general theory of the light-activated interfacial self-healing to soft polymers with organic photophores. Unlike the soft polymers crosslinked by multifunctional nanomaterials, the organic crosslinker cannot bridge a large number of polymer chains. To consider the inhomogeneous chain length distribution, we employ an interpenetration network model that assumes the polymer is composed of *m* types of networks interpenetrating in the material bulk (Fig. 6a) (Wang et al., 2015). In each network, the chain length is the same, denoted as n_1, n_2, ... and n_m. In the undeformed state, all chains are freely-joint; therefore, the end-to-end distance of the *i*th chain is

$$L_i = \sqrt{n_i}b \tag{35}$$

With the chain number of the *i*th chain per unit volume as N_i, we can also express the chain length distribution as Eq. (21).

With the affined deformation model, the stretch of the *i*th chain is different from Eq. (26), but should be

$$\Lambda_i = \sqrt{\frac{\lambda_1^2 + \lambda_2^2 + \lambda_3^2}{3}} \tag{36}$$

With the strain energy density expressions of the original material similar to Eq. (30), we can write the uniaxial nominal stresses of the original material as

$$s_1 = \frac{(\lambda - \lambda^{-2})k_B T}{\sqrt{3\lambda^2 + 6\lambda^{-1}}} \sum_{i=1}^{m} \left[N_i^a \sqrt{n_i} L^{-1} \left(\sqrt{\frac{\lambda^2 + 2\lambda^{-1}}{3n_i}} \right) \right] \tag{37}$$

Then, following the similar microscopic picture as self-healing of the nanocomposite hydrogels shown in Fig. 5d, we can model the behavior of the self-healed segment of the soft polymers with organic photophores in Fig. 6b. The corresponding uniaxial nominal stress of the self-healed segment can be written as

$$s_1^h = \frac{\left(\lambda^h - \lambda^{h-2}\right)k_B T}{\sqrt{3\lambda^{h2} + 6\lambda^{h-1}}} \sum_{i=1}^{m} \left[N_i^{ah} \sqrt{n_i} L^{-1} \left(\sqrt{\frac{\lambda^{h2} + 2\lambda^{h-1}}{3n_i}} \right) \right] \tag{38}$$

Going through the calculation process shown in Section 3.2, we can calculate the stress–strain behaviors of the self-healed samples and the corresponding healing strength for various healing time (results in Section 5).

4. Results for light-activated self-healing polymers with inorganic photophores

In this section, we will first take the photo-healable TiO_2 nanocomposite hydrogel as an example to illustrate how to relate the light property to the interfacial self-healing performance. We will also examine the effects of light intensity and light wavelength on the self-healing performance. The theoretical results will be compared with the experimental ones. All used parameters are presented in Table 1.

Table 1

Definition and value of the employed parameters. The initial light intensity for Figs. 7–11 are directly extracted from experiments. The initial light intensity for Figs. 13–15 is estimated by $P/(4\pi L^2)$, where the power $P = 14\,w$ and $L = 20\,cm$ is the distance between the lamp and the sample (Amamoto et al., 2012). The absorption coefficient of the material matrix of partially opaque TiO2 hydrogel follows the one of the optically thick polymer discussed in (Long et al., 2009; Zhao et al., 2015), and the absorption coefficient of the material matrix of clear polymers in (Amamoto et al., 2012) follows the one of the optically thin polymer discussed in (Long et al., 2009; Zhao et al., 2015). The number of radicals produced per TiO$_2$ nanoparticle photoinitiator in Figs. 7–11 is estimated as in the same order of the active binding sites N_{site} on the nanoparticle surfaces. As $N_{site} = 4r^2\kappa/b^2$, where b is the Kuhn segment length, r is the particle radius, and κ is the particle activity parameter (Bueche, 1960; Wang and Gao, 2016). Following (Wang and Gao, 2016), we estimate κ is in the order of 0.01; then, we roughly estimate the binding site number is in the order of 10^3. Therefore, we estimate the number of radicals produced per TiO$_2$ nanoparticle photoinitiator in Figs. 7–11 as 1000. Forward and reverse reaction rates are estimated from the ones for the dynamic covalent bonding kinetics in (Yu et al., 2018b). n_a is a fitting parameter used to match the stress–strain behaviors of original polymer networks. Δx is another fitting parameter used to match the tensile strength of original polymer networks (Wang and Gao, 2016; Wang et al., 2017; Yu et al., 2018b). The rouse friction coefficient is the third fitting parameter to match the healing time-scale (Wang et al., 2017; Yu et al., 2018b).

| Parameter	Definition	Figs. 7–9	Fig. 10	Fig. 11	Figs. 13 and 15	Fig. 14	Estimation source
I_0 (W m^{-2})	Initial light intensity	37	7.4-37	37	27.9	27.9	Experimental data
α_1 (m^3 mol^{-1} s^{-1})	Molar absorptivity of the photoinitiator	N/A	N/A	N/A	0.1	0.1	Long et al. (2009), Zhao et al. (2015)
A_{mat} (m^{-1})	Absorption coefficient of the material matrix	120	120	120	10	10	Long et al. (2009), Zhao et al. (2015)
α_2 (m^2 W^{-1} s^{-1})	Light absorption coefficient for the radical production	2.65×10^{-5}	2.65×10^{-5}	2.65×10^{-5} & 1.25×10^{-5}	3.51×10^{-8}	3.51×10^{-8}	Long et al. (2009), Ma et al. (2014), Zhao et al. (2015)
n_R	Number of radicals produced per photoinitiator	1000	1000	1000	2	2	Bueche (1960), Wang and Gao (2016)
D_R (m^2 s^{-1})	Diffusivity of the radical	1×10^{-10}	1×10^{-10}	1×10^{-10}	1×10^{-10}	1×10^{-10}	Long et al. (2009), Zhao et al. (2015)
k_t (s^{-1} mol^{-1} m^3)	Termination rate of the radical	0.1	0.1	0.1	0.1	0.1	Long et al. (2009), Zhao et al. (2015)
D_I (m^2 s^{-1})	Diffusivity of organic photoinitiator	N/A	N/A	N/A	1×10^{-10}	1×10^{-10}	Long et al. (2009), Zhao et al. (2015)
η (mol m^{-3})	Volume concentration of nanocrosslinker	2.33×10^{-3}	2.33×10^{-3}	2.33×10^{-3}	N/A	N/A	Experimental data
C_{I0} (mol m^{-3})	Initial photoinitiator concentration	η	η	η	0.5	0.01-1	Experimental data
k_1 (s^{-1} mol^{-2} m^6)	Coefficient for the forward reaction rate	0.5	0.5	0.5	5	5	Wang et al. (2017), Yu et al. (2018b)
k_i^{r0} (s^{-1})	Reverse reaction rate	2×10^{-6}	2×10^{-6}	2×10^{-6}	2×10^{-6}	2×10^{-6}	Wang et al. (2017), Yu et al. (2018b)
Δx(m)	Distance along the energy landscape coordinate	4×10^{-9}	4×10^{-9}	4×10^{-9}	5.1×10^{-9}	5.1×10^{-9}	Fitting parameter
b (m)	Kuhn segment length	5.2×10^{-10}	5.2×10^{-10}	5.2×10^{-10}	5.2×10^{-10}	5.2×10^{-10}	Wang et al. (2017), Yu et al. (2018b)
n_1	Minimum chain length	300	300	300	100	100	Chosen based on n_a
n_m	Maximum chain length	1500	1500	1500	800	800	Chosen based on n_a
n_a	Average chain length	576	576	576	400	400	Fitting parameter
δ	Chain length distribution width	0.15	0.15	0.15	0.2	0.2	Wang and Gao (2016), Wang et al. (2017), Yu et al. (2018b)
ξ(N/m)	Rouse friction coefficient	5×10^{-8}	5×10^{-8}	5×10^{-8}	5×10^{-5}	5×10^{-5}	Fitting parameter
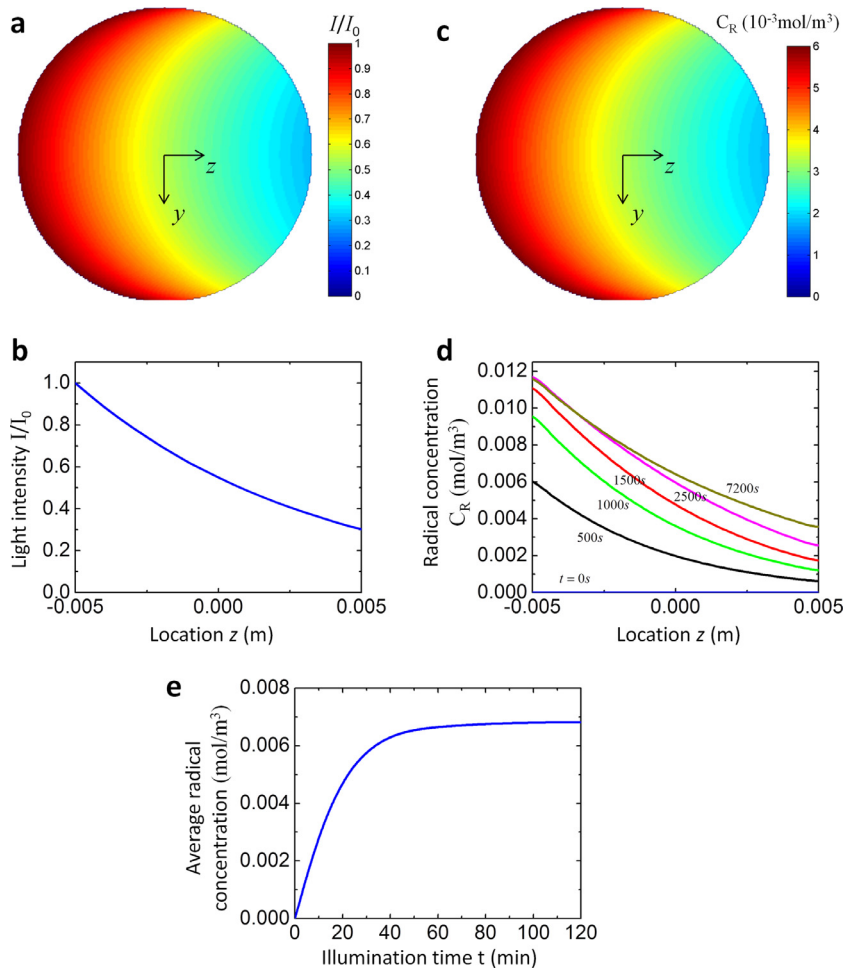
Fig. 7. Photoinitiation within the TiO$_2$ nanocomposite hydrogel. (a) The light intensity distribution on the healing interface. (b) The light intensity distribution along the depth z. (c) The radical concentration distribution on the healing interface at illumination time $t = 500$ s. (d) The radical concentration C$_R$ as functions of the depth z for various light illumination time t. (e) The average radical concentration on the healing interface as a function of light illumination time t.

4.1. Results for the light propagation within the TiO$_2$ nanocomposite hydrogel

As shown in Fig. 1b–e, the TiO$_2$ nanocomposite hydrogel is partially opaque; therefore, the absorption coefficient of the material matrix is much larger than the absorption induced by the photoinitiator, i.e., $\alpha_1 C_I(\mathbf{x}, t) \ll A_{mat}$. We thus solve the light intensity distribution as (Fig. 3c)

$$I(z) \approx I_0 \exp\left[-A_{mat}\left(\sqrt{r^2 - y^2} + z\right)\right] \tag{39}$$

where I_0 is the initial light intensity and r is the radius of the cross-section area. The light intensity distribution in the cross-section region is shown in Fig. 7a. The corresponding light intensity along the central line is plotted in Fig. 7b. This light intensity distribution will not change during the whole light-activation process.

As for the TiO$_2$ nanocomposite hydrogel, the photoinitiator is the TiO$_2$ nanoparticle whose concentration does not change during the whole light-activation process; thus, we have $C_I = \eta$ in Eq. (3). Solving Eq. (3) leads to the concentration distributions of the free radical in the cross-section region (Fig. 7c). With increasing illumination time, more and more free radicals are produced on the cross-section region (Fig. 7d). Note that the concentration distribution of the free radical is inhomogeneous over the cross-section area: more radicals are produced at the locations closer to the light incident surface. It means that the healing percentage will vary across the interface. To simplify the problem, we average the radical concentration across the interface as $\overline{C_R}(t)$ (Fig. 7e) and consider an effectively homogeneous self-healing across the interface in Section 4.2.
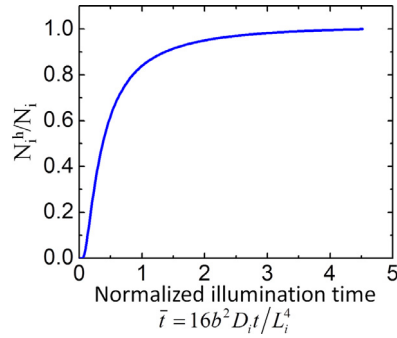
Fig. 8. The effective concentration of the linked ith chain within the healed region as a function of normalized UV illumination time.
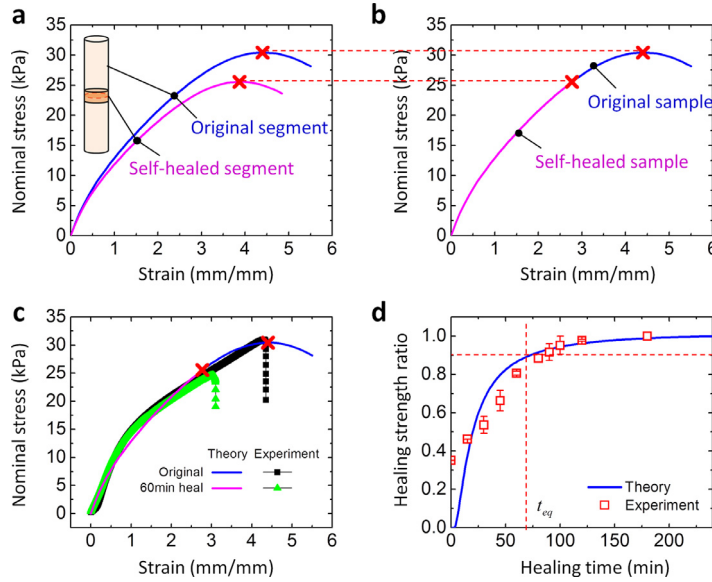

Fig. 9. (a) The nominal stresses of the original and self-healed segments as functions of uniaxial strains of these segments. (b) The nominal stresses of the original and self-healed samples as functions of uniaxial strains of these samples. (c) The comparisons between the experimentally measured and theoretically calculated nominal stress–strain behaviors of the original and self-healed nanocomposite hydrogel samples. (d) The experimentally measured and theoretically calculated healing strength ratios of the nanocomposite hydrogel as functions of the healing time.

4.2. Results for the penetration of the ith chain

Once the average radical concentration in the cross-section area is calculated, we can employ Eqs. (13) and (17) and related boundary and initial conditions Eqs. (14–16) to calculate the average ith chain number density N_i^h within the self-healed region (Fig. 8). Note that the radical concentration $C_R(\mathbf{x}, t)$ will be replaced by the time-dependent average radical concentration in the cross-section area $\overline{C}_R(t)$. As seen from Fig. 8, the average ith chain density $N_i^h(t)$ increases from zero to reach a plateau N_i as the time is long enough. The time scale to reach the plateau depends on the Rouse diffusivity of the ith chain D_i and the free radical concentration $\overline{C}_R(t)$.

4.3. Results for the light-activated self-healing of soft polymers with nanomaterial photophore

The self-healed sample has three segments: two segments with original materials and one small self-healed segment with the re-formed linked ith chains (see inset of Fig. 9a). Once the healed linked ith chain density within the self-healing region is calculated, we can employ the interpenetration network model shown in Section 3.2 to calculate the stress–strain behaviors of the original and the self-healed segments, respectively (Fig. 9a). Note that the stress–strain curve of the original material features a maximum that is considered as the tensile strength of the material (Fig. 9a). For an original hydrogel sample, as the nominal stress gradually increases with the stretch, the polymer chains are gradually detached from the nanoparticles (Fig. 5c). Once most of the polymer chains are detached, the nominal stress begins to decrease. At the critical point (denoted by the red cross on the blue line in Fig. 9a), the hydrogel sample breaks into two parts, and the red cross indicates the tensile strength of the hydrogel. In the following, we will employ the tensile strength as the indicator for the
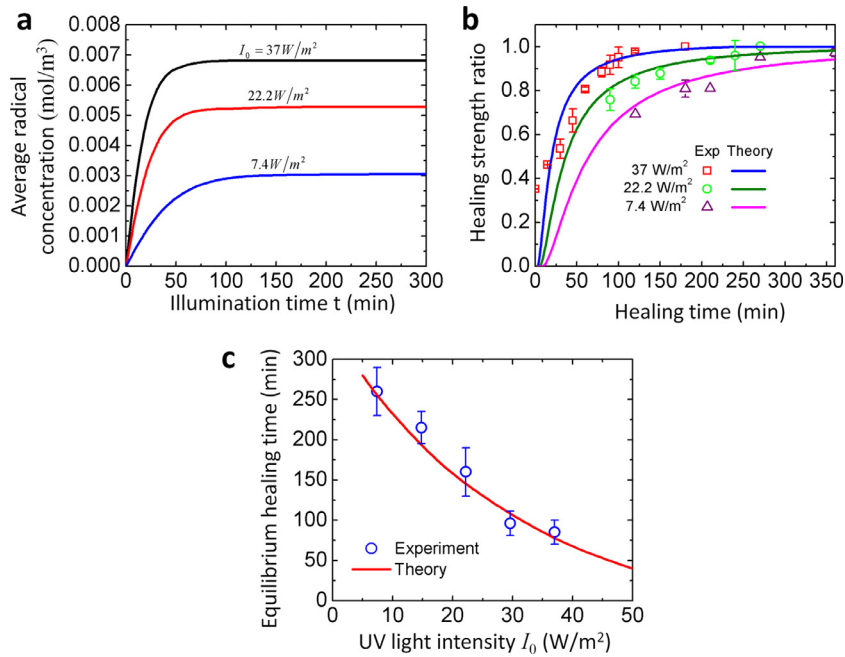
Fig. 10. Effect of the light intensity on the self-healing behavior of the TiO$_2$ nanocomposite hydrogel. (a) The average radical concentrations on the healing interface for various initial UV light intensities as functions of the UV illumination time. (b) The experimentally measured and theoretically calculated healing strength ratios of the TiO$_2$ nanocomposite hydrogels for various UV intensities as functions of healing time. (c) The experimentally measured and theoretically calculated equilibrium healing time as functions of the UV light intensity.

interfacial healing. The major reason is that the measurement of the interfacial strength in experiments is relatively easy and most of the researchers in the self-healing community use the tensile strength in their experiments (Blaiszik et al., 2010; Burattini et al., 2010; Wojtecki et al., 2011; Wool, 2008; Wu et al., 2008; Yang and Urban, 2013). The results of interfacial strength are reliable when the sample number is large enough to eliminate the effects of small defects. In the experiments, we always use multiple samples (up to 10 samples for each case) to validate the accuracy of the measurement.

We assume undeformed and deformed lengths of the self-healed segment are H^h and h^h, respectively, and the corresponding undeformed and deformed lengths of the sample are H and h, respectively. The stretch of the original segment is calculated as

$$\frac{h - h^h}{H - H^h} \approx \frac{h}{H} \tag{40}$$

because $h \gg h^h$ and $H \gg H^h$; therefore, the stretch of the self-healed sample is approximately the same as the stretch of the original segment. As nominal stresses in the original segment and the self-healed segment should be equal ($s_1^h = s_1$), we can predict that the stress–strain curve of the self-healed sample follows the trace of the stress–strain curve of the original sample, only with a lower maximal nominal stress (indicated as the red cross in Fig. 9b). This can be validated by the experimentally measured stress–strain behaviors of the self-healed sample (Fig. 9c). Collecting the maximal nominal stress (named as healing strength) corresponding to each healing time, we can predict the relationship between the healing strength as a function of the healing time (Fig. 9d). To present the results, we usually normalize the healing strength with the uniaxial strength of the original material and calculate as healing strength ratio (Fig. 9d). We find the healing strength ratio increases with increasing the healing time and reaches a plateau when the healing time is long enough. To indicate the healing speed, we denote the equilibrium healing time as the time corresponding to 90% healing strength ratio. We find that the theoretically calculated relationship between the healing strength ratio can roughly match with the experimental results of the light-activated self-healing of the TiO$_2$ nanocomposite hydrogels (Fig. 9d). The discrepancy exists in the short healing time range because the theoretical model does not take the immediate adhesion into account. More discussions about this limitation can be found in the conclusive remarks.

4.3.1. Effect of light intensity

To illustrate the capability of our theoretical model, we then study the effect of light intensity on the self-healing performance of the TiO$_2$ nanocomposite hydrogels (Fig. 10). With the higher initial UV light intensity I_0, the average radical concentration on the healing interface reaches the higher plateau within a shorter light illumination time (Fig. 10a). According to Eq. (13), the higher concentration of radicals will promote the binding reactions between the distal groups and binding sites, and thus accelerate the healing process. Therefore, the predicted healing strength ratios reach the plateau within a
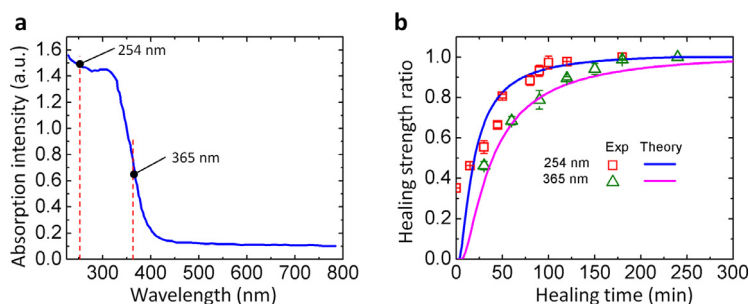
Fig. 11. Effect of the UV wavelength on the self-healing behaviors of the TiO$_2$ nanocomposite hydrogel. (a) The absorption spectrum of the TiO$_2$ nanoparticles. The curve is reproduced from reference (Huang et al., 2012) with permission. (b) The healing strength ratio of the TiO$_2$ nanocomposite hydrogel under UV light 254 nm and 365 nm as functions of the healing time.
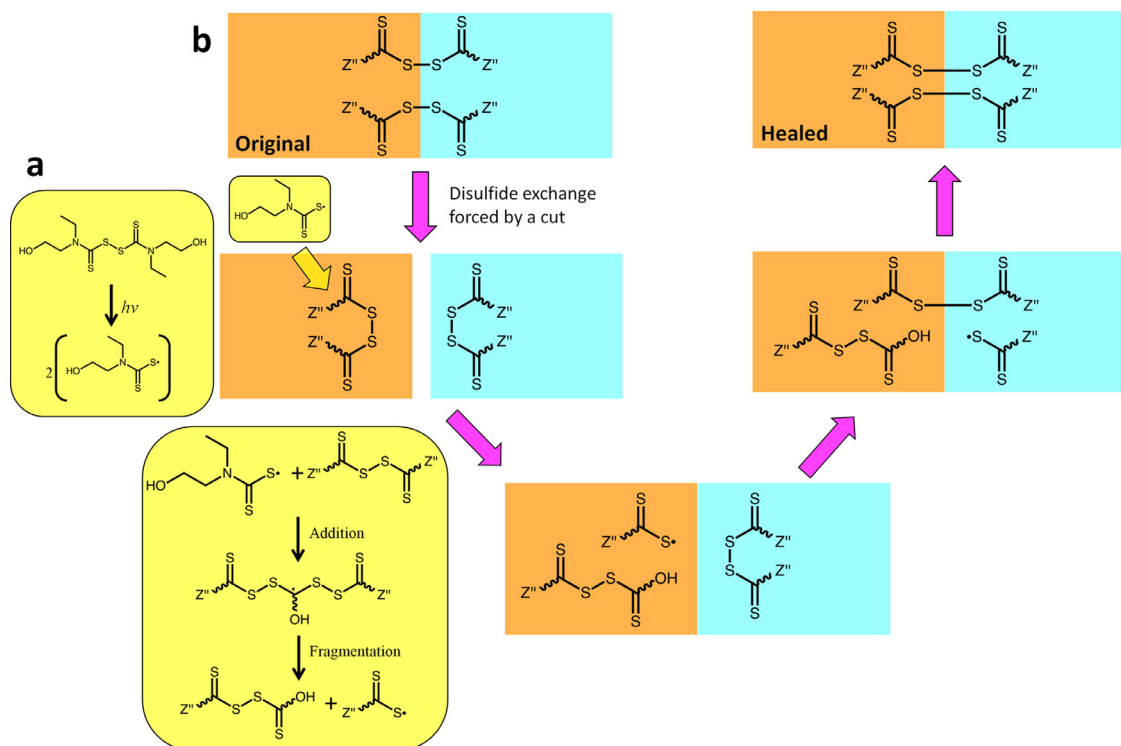

Fig. 12. (a) The light-induced homolytic cleavage reaction of the thiuram disulfide (TDS) diol to produce free radicals. (b) Reaction process around the healing interface of the light-activated healable polymers with thiuram disulfide (TDS) moieties. The TDS radicals transfer across the interface to rebridge the fractured interface.

shorter healing time for the higher light intensity cases (Figs. 10b and 1f). In addition, we show that the theoretically calculated healing strength ratio and equilibrium healing time can consistently match with the corresponding experimental results (Fig. 10c).

4.3.2. Effect of light wavelength

To further illustrate the capability of the theoretical model, we study the effect of UV wavelength on the self-healing performance of the TiO$_2$ nanocomposite hydrogels (Fig. 11). The activities of TiO$_2$ nanoparticles vary for different wavelengths of the incident light. The absorption intensities of the employed TiO$_2$ nanoparticle for various incident light wavelength is shown in Fig. 11a (Huang et al., 2012). The absorption coefficient α_2 in Eq. (3) is expected to be proportional to the absorption intensity of the TiO$_2$ nanoparticle. From Fig. 11a, we can estimate that $\alpha_2^{365}/\alpha_2^{254} \approx 2.12$, where α_2^{365} and α_2^{254} are the absorption coefficient of the TiO$_2$ nanoparticle for UV lights with wavelengths 365 nm and 254 nm, respectively. Based on the theoretical calculation for 254 nm UV light, we can predict the relationship between the healing strength ratio and the healing time for 365 nm UV light (Fig. 11b). The theoretical results match consistently with the experimentally measured ones.
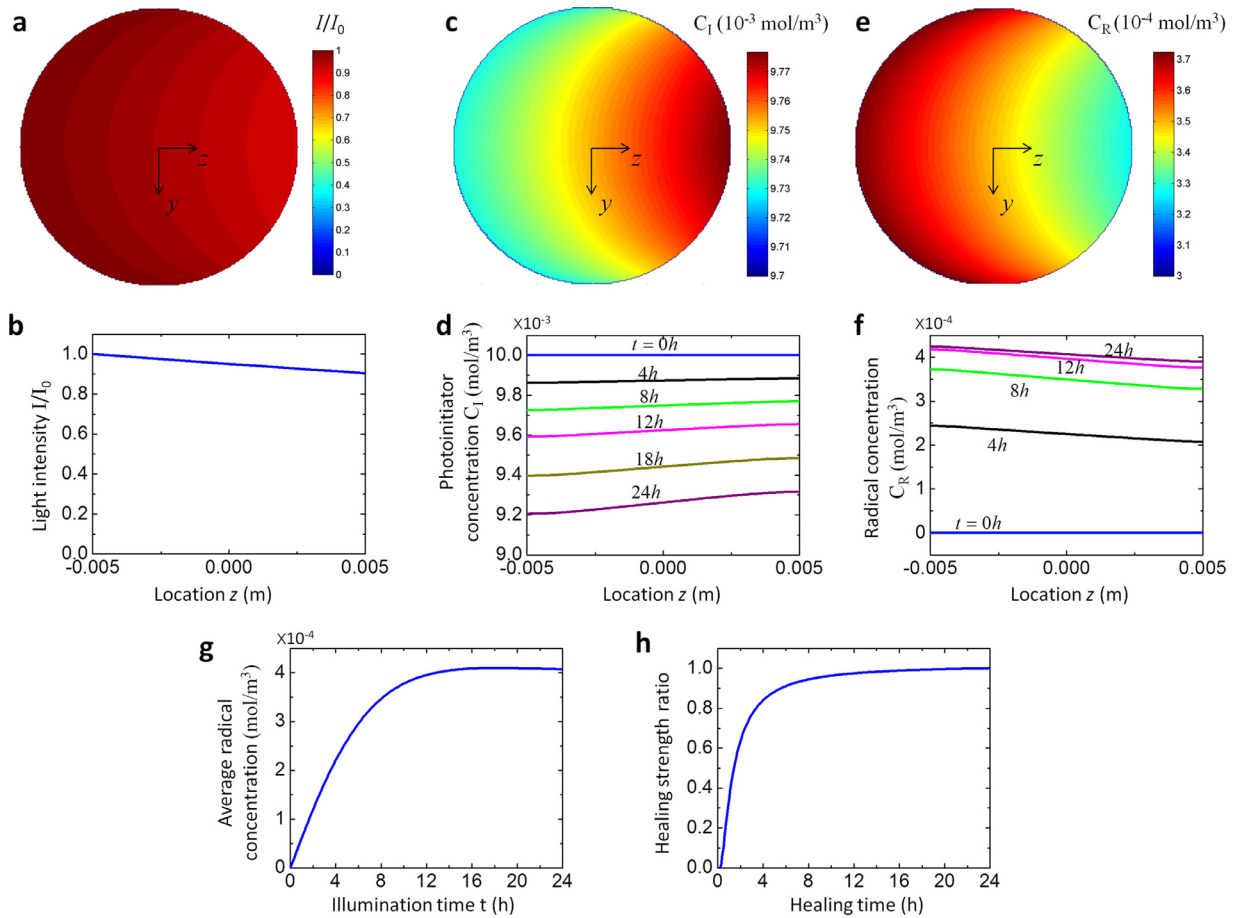
Fig. 13. (a) The light intensity distribution on the healing interface. (b) The light intensity distribution along the depth z on the healing interface. (c) The photoinitiator concentration distribution on the healing interface at $t = 8$ h. (d) The photoinitiator concentration C_I as functions of the depth z for various light illumination time t. (e) The radical concentration distribution on the healing interface at $t = 8$ h. (f) The radical concentration C_R as functions of the depth z for various light illumination time t. (g) The average radical concentration on the healing interface as a function of light illumination time t. (h) The healing strength ratio as a function of healing time of the polymer with organic photophores.

5. Results for light-activated self-healing polymers with organic photophores

In this section, we show that the theory can also be used to explain the light-activated self-healing of soft polymers with organic photophores. The effect of photoinitiator concentration on the self-healing performance is examined. The theoretical calculations of the self-healing performance of the soft polymers with organic photophores are compared with the experimentally measured results. All used parameters are presented in Table 1.

Here, we consider a light-activated healable polymer system in (Amamoto et al., 2012) (Fig. 12). The thiuram disulfide (TDS) unit can undergo a light-induced homolytic cleavage reaction to produce free radicals (Amamoto et al., 2011, 2012; Degirmenci and Coote, 2016). This TDS unit can be within a crosslinked polymer network or the TDS diol. The TDS diol comes from the unreacted TDS diol during the polymer synthesis. Since the mobility of the TDS unit within the crosslinked polymer network is very limited, the mobile TDS diols are anticipated to contribute the majority mobile free radicals during the light-activated self-healing process. Therefore, we believe that the TDS diol serves as the major photoinitiator. Under light actuation, the TDS diol is decomposed into two free TDS radicals (Fig. 12a). Then, the TDS radicals transfer across the interface to re-bridge the fractured interface (Fig. 12b) (Amamoto et al., 2011, 2012; Degirmenci and Coote, 2016).

For the TiO$_2$ nanocomposite hydrogel, TiO$_2$ nanoparticles serve as the photoinitiator, and its concentration does not change during the light-activation process. However, for the soft polymers with organic photophores, the concentration of the initial organic photoinitiator will decrease during the light illumination process. The photoinitiators will be decomposed into free radicals to activate the self-healing process. As for a sample in a circular bar shape, three fields are coupled within the circular healing interface: the light intensity Eq. (1), the photoinitiator concentration Eq. (3), and radical concentration Eq. (4). We employ the numerical software COMSOL with its general PDE function to solve the coupled fields. As shown in Fig. 13a and b, the light intensity decreases from the incident surface to the rear surface. Higher light intensity consumes
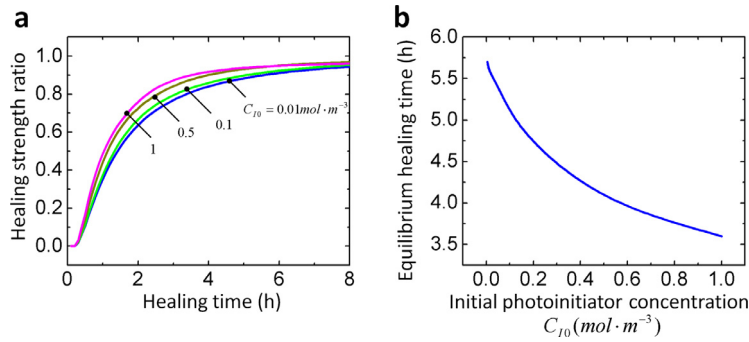
Fig. 14. Effect of photoinitiator concentration on the self-healing behavior of the polymer with organic photophores. (a) The healing strength ratios for various initial photoinitiator concentrations as functions of the healing time. (b) The equilibrium healing time as a function of the initial photoinitiator concentration.
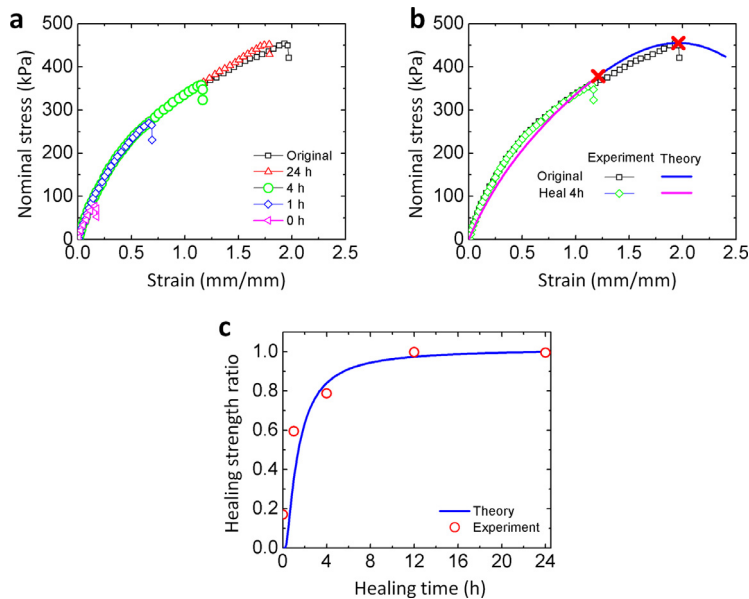

Fig. 15. (a) The experimentally measured nominal stress–strain behaviors of the original and self-healed polymers with organic photophores. (b) The comparisons between the experimentally measured and theoretically calculated nominal stress–strain behaviors of the original and self-healed polymers with organic photophores. (c) The experimentally measured and theoretically calculated healing strength ratios as functions of the healing time. The results in (a-c) are reproduced from (Amamoto et al., 2012) with permission.

more photoinitiators to produce more radicals; therefore, the photoinitiator concentration is lower at the incident surface (Fig. 13c and d), while the radical concentration is higher at the incident surface (Fig. 13e and f). As the light illumination time increases, the overall photoinitiator concentration decreases but the radical concentration increases. Similar to the TiO_2 nanocomposite hydrogel, we consider an effectively homogenous self-healing over the healing interface. We thus calculate the average radical concentration as a function of the illumination time (Fig. 13g). We find that the average radical concentration first increases with the increasing illumination time and then reaches a plateau. This plateau is because of the saturation of radical production. Then, with the average radical concentration, we follow the model shown in Section 3.3 to calculate the relationship between the healing strength ratio and the healing time for the soft polymer with organic photophores (Fig. 13h).

5.1. Effect of photoinitiator concentration

With the above method, we can predict the effect of the initial photoinitiator concentration C_{I0} on the self-healing behavior of the soft polymer with organic photophores (Fig. 14). Higher photoinitiator concentration induces the higher average radical concentration on the healing interface. And higher radical concentration leads to the faster healing process of the material (Fig. 14a and b). Therefore, the equilibrium healing time decreases with increasing initial photoinitiator concentration (Fig. 14b). Besides, we find that the changing rate of the equilibrium healing time is decreasing with increasing photoinitia-

tor concentration. It is because the radical production is close to the saturation state when the photoinitiator concentration is high, and the equilibrium healing time change is less insensitive than that when the photoinitiator concentration is low.

To verify the theoretical model, we compare the theoretical results with the experimentally measured results for a polymer with organic photophores thiuram disulfide moieties (Amamoto et al., 2012). This polymer can self-heal the interfacial strength by around 100% with the illumination of visible light for 24 h (Fig. 15a). Using the developed theory in Section 3.3, we can plot the uniaxial nominal stress–strain behaviors for the original and self-healed polymer samples, which agree well with the experimentally measured results. The theoretically calculated relationship between the healing strength ratio and the healing time also match the experimental results. Note that the theoretical calculations for Fig. 15 follow the method discussed around Fig. 13. The cross-section shape of the sample here is rectangular (2 mm x 1 mm). As we actually homogenize the chemical concentrations across the interface, the cross-section shape has little influence on the healing strength. To be consistent, we still roughly approximate the cross-section as a circle (radius 0.8 mm) for the case in Fig. 15. We predict that the equilibrium healing time with 90% healing strength is around 6 h, while this specific number is usually challenging to determine in the experiment without carefully screening over the whole hour range.

6. Conclusive remarks

In summary, we present a theoretical framework to understand the light-activated interfacial self-healing of soft polymers with both inorganic and organic photophores. We consider that the light within the material matrix triggers the production of free radicals that further facilitate the interfacial self-healing process. The self-healing process is considered as a coupled phenomenon that polymer chains diffuse across the interface and re-form the dynamic bonds assisted by the free radicals. We theoretically relate the light property and the interfacial self-healing strength of the polymers. We predict that the interfacial self-healing strength of the polymer increases with the light illumination time until reaching a plateau. We study the effects of the light intensity, light wavelength, and photoinitiator concentration on the self-healing performance. We apply the theory to two types of soft polymers with inorganic and organic photophores, respectively. The experimentally measured stress–strain behaviors of the original and self-healed samples can be consistently explained by the theory. The theoretically calculated relationships between the healing strength and the healing time can also agree well with the experiments. Though mechanics models for the constitutive behaviors of light-activated polymers have been proposed (Long et al., 2011, 2009, 2013; Ma et al., 2014), to the best of our knowledge, this paper presents the first network-based theory for the light-activated self-healing mechanics. The major contribution of the current work is a theoretical framework to integrate the light-triggered free radical production and the interfacial polymer chain evolution.

Despite the contribution to the mechanics field, this theoretical framework also leaves several open questions. First, we have not considered the immediate interfacial adhesion in this theoretical framework. As shown in Figs. 9–11 and 14, the immediate adhesion may lead to around 20–35% of interfacial strength. The immediate adhesion process has a time scale much shorter than the healing process. However, this paper considers that only the re-binding of the open chains can sustain the load, and the immediate adhesion of the fractured interface is considered to be around zero. We conservatively think that it may not be fully correct if we simply add the immediate adhesion strength and healing strength as they dominate at different time-scales. Second, we only consider the light-assistance on the self-healing performance is because the light-produced radicals facilitate the binding process. In the experiments without special treatment, the temperature of the material matrix increases slightly during the light illumination process. This temperature increase may also accelerate the chain diffusion and chain re-binding. To mitigate this issue, in our experiments of TiO_2 nanocomposite hydrogels, we maintain the material temperature within a thermal incubator with a constant temperature 25 °C. In the future, more careful experiments should be carried out to characterize the material temperature change during the self-healing process, because the temperature is an important factor to affect the self-healing speed. Third, the paper may be further extended to explain light-assisted self-healing processes that have not covered in this paper. For example, Weder, et al. reported optically healable plastics (Balkenende et al., 2016; Burnworth et al., 2011b; Fiore et al., 2013). Though the current paper focuses on the deformable soft polymer networks, adding the plastic deformation mechanism may further extend the theory to optically healable plastics.

Acknowledgements

Supplementary material

Supplementary material associated with this article can be found, in the online version, at doi:10.1016/j.jmps.2018.11.019.

Reference

Amamoto, Y., Kamada, J., Otsuka, H., Takahara, A., Matyjaszewski, K., 2011. Repeatable photoinduced self-healing of covalently cross-linked polymers through reshuffling of trithiocarbonate units. Angew. Chemie Int. Ed. 50, 1660–1663.

Amamoto, Y., Otsuka, H., Takahara, A., Matyjaszewski, K., 2012. Self-healing of covalently cross-linked polymers by reshuffling thiuram disulfide moieties in air under visible light. Adv. Mater. 24, 3975–3980.

Balkenende, D.W., Monnier, C.A., Fiore, G.L., Weder, C., 2016. Optically responsive supramolecular polymer glasses. Nat. Commun. 7, 10995.

Bell, G.I., 1978. Models for the specific adhesion of cells to cells. Science 200, 618–627.

Bhattacharya, S., Samanta, S.K., 2016. Soft-nanocomposites of nanoparticles and nanocarbons with supramolecular and polymer gels and their applications. Chem. Rev. 116, 11967–12028.

Blaiszik, B., Kramer, S., Olugebefola, S., Moore, J.S., Sottos, N.R., White, S.R., 2010. Self-healing polymers and composites. Annu. Rev. Mater. Res. 40, 179–211.

Brochu, A.B., Craig, S.L., Reichert, W.M., 2011. Self-healing biomaterials. J. Biomed. Mater. Res. Part A 96, 492–506.

Bueche, F., 1960. Molecular basis for the Mullins effect. J. Appl. Polym. Sci. 4, 107–114.

Burattini, S., Greenland, B.W., Chappell, D., Colquhoun, H.M., Hayes, W., 2010. Healable polymeric materials: a tutorial review. Chem. Soc. Rev. 39, 1973–1985.

Burnworth, M., Tang, L., Kumpfer, J.R., Duncan, A.J., Beyer, F.L., Fiore, G.L., Rowan, S.J., Weder, C., 2011a. Optically healable supramolecular polymers. Nature 472, 334–337.

Burnworth, M., Tang, L., Kumpfer, J.R., Duncan, A.J., Beyer, F.L., Fiore, G.L., Rowan, S.J., Weder, C., 2011b. Optically healable supramolecular polymers. Nature 472, 334.

Chen, X., Dam, M.A., Ono, K., Mal, A., Shen, H., Nutt, S.R., Sheran, K., Wudl, F., 2002. A thermally re-mendable cross-linked polymeric material. Science 295, 1698–1702.

Chen, Y., Kushner, A.M., Williams, G.A., Guan, Z., 2012. Multiphase design of autonomic self-healing thermoplastic elastomers. Nat. Chem. 4, 467–472.

Cho, S.H., Andersson, H.M., White, S.R., Sottos, N.R., Braun, P.V., 2006. Polydimethylsiloxane-based self-healing materials. Adv. Mater. 18, 997–1000.

Cordier, P., Tournilhac, F., Soulié-Ziakovic, C., Leibler, L., 2008. Self-healing and thermoreversible rubber from supramolecular assembly. Nature 451, 977–980.

De Gennes, P.-G., 1979. Scaling Concepts in Polymer Physics. Cornell University Press.

de Gennes, P.G., 1971. Reptation of a polymer chain in the presence of fixed obstacles. J. Chem. Phys. 55, 572–579.

Degirmenci, I., Coote, M.L., 2016. Understanding the behaviour of sulphur-centred radicals during polymer self-healing. J. Turk. Chem. Soc. Sect. A 3, 707–720.

Doi, M., Edwards, S.F., 1978. Dynamics of concentrated polymer systems. Part 1.– Brownian motion in the equilibrium state. J. Chem. Soc. Faraday Trans. 74, 1789–1801.

Doi, M., Edwards, S.F., 1988. The Theory of Polymer Dynamics. Oxford University Press.

Fiore, G.L., Rowan, S.J., Weder, C., 2013. Optically healable polymers. Chem. Soc. Rev. 42, 7278–7288.

Froimowicz, P., Frey, H., Landfester, K., 2011. Towards the generation of self-healing materials by means of a reversible photo-induced approach. Macromol. Rapid Commun. 32, 468–473.

Ghosh, B., Urban, M.W., 2009. Self-repairing oxetane-substituted chitosan polyurethane networks. Science 323, 1458–1460.

Habault, D., Zhang, H., Zhao, Y., 2013. Light-triggered self-healing and shape-memory polymers. Chem. Soc. Rev. 42, 7244–7256.

Haraguchi, K., 2007. Nanocomposite hydrogels. Curr. Opin. Solid State Mater. Sci. 11, 47–54.

Haraguchi, K., 2011. Synthesis and properties of soft nanocomposite materials with novel organic/inorganic network structures. Polym. J. 43, 223–241.

Haraguchi, K., Takehisa, T., 2002. Nanocomposite hydrogels: a unique organic – inorganic network structure with extraordinary mechanical, optical, and swelling/de-swelling properties. Adv. Mater. 14, 1120–1124.

Haraguchi, K., Uyama, K., Tanimoto, H., 2011. Self-healing in nanocomposite hydrogels. Macromol. Rapid Commun. 32, 1253–1258.

Holten-Andersen, N., Harrington, M.J., Birkedal, H., Lee, B.P., Messersmith, P.B., Lee, K.Y.C., Waite, J.H., 2011. pH-induced metal-ligand cross-links inspired by mussel yield self-healing polymer networks with near-covalent elastic moduli. Proc. Natl. Acad. Sci. USA 108, 2651–2655.

Hu, Z., Chen, G., 2014. Novel Nanocomposite hydrogels consisting of layered double hydroxide with ultrahigh tensibility and hierarchical porous structure at low inorganic content. Adv. Mater. 26, 5950–5956.

Huang, K., Chen, L., Deng, J., Xiong, J., 2012. Enhanced visible-light photocatalytic performance of nanosized anatase TiO_2 doped with CdS quantum dots for cancer-cell treatment. J. Nanomater. 2012, 11.

Ji, S., Cao, W., Yu, Y., Xu, H., 2015. Visible-light-induced self-healing diselenide-containing polyurethane elastomer. Adv. Mater. 27, 7740–7745.

Keller, M.W., White, S.R., Sottos, N.R., 2007. A self-healing poly (Dimethyl Siloxane) elastomer. Adv. Funct. Mater. 17, 2399–2404.

Kim, Y.H., Wool, R.P., 1983. A theory of healing at a polymer-polymer interface. Macromolecules 16, 1115–1120.

Ling, J., Rong, M.Z., Zhang, M.Q., 2012. Photo-stimulated self-healing polyurethane containing dihydroxyl coumarin derivatives. Polymer 53, 2691–2698.

Liu, M., Ishida, Y., Ebina, Y., Sasaki, T., Aida, T., 2013. Photolatently modulable hydrogels using unilamellar titania nanosheets as photocatalytic crosslinkers. Nat. Commun. 4, 2029.

Liu, M., Ishida, Y., Ebina, Y., Sasaki, T., Hikima, T., Takata, M., Aida, T., 2015. An anisotropic hydrogel with electrostatic repulsion between cofacially aligned nanosheets. Nature 517, 68.

Long, K.N., Scott, T.F., Dunn, M.L., Jerry Qi, H., 2011. Photo-induced deformation of active polymer films: single spot irradiation. Int. J. Solids Struct. 48, 2089–2101.

Long, K.N., Scott, T.F., Qi, H.J., Bowman, C.N., Dunn, M.L., 2009. Photomechanics of light-activated polymers. J. Mech. Phys. Solids 57, 1103–1121.

Long, R., Qi, H.J., Dunn, M.L., 2013. Thermodynamics and mechanics of photochemcially reacting polymers. J. Mech. Phys. Solids 61, 2212–2239.

Ma, J., Mu, X., Bowman, C.N., Sun, Y., Dunn, M.L., Qi, H.J., Fang, D., 2014. A photoviscoplastic model for photoactivated covalent adaptive networks. J. Mech. Phys. Solids 70, 84–103.

Mayumi, K., Guo, J., Narita, T., Hui, C.Y., Creton, C., 2016. Fracture of dual crosslink gels with permanent and transient crosslinks. Extreme Mech. Lett. 6, 52–59.

Michal, B.T., Jaye, C.A., Spencer, E.J., Rowan, S.J., 2013. Inherently photohealable and thermal shape-memory polydisulfide networks. ACS Macro Lett. 2, 694–699.

Nakahata, M., Takashima, Y., Yamaguchi, H., Harada, A., 2011. Redox-responsive self-healing materials formed from host – guest polymers. Nat. Commun. 2, 511.

Otsuka, H., Nagano, S., Kobashi, Y., Maeda, T., Takahara, A., 2010. A dynamic covalent polymer driven by disulfide metathesis under photoirradiation. Chem. Commun. 46, 1150–1152.

Phadke, A., Zhang, C., Arman, B., Hsu, C.-C., Mashelkar, R.A., Lele, A.K., Tauber, M.J., Arya, G., Varghese, S., 2012. Rapid self-healing hydrogels. Proc. Natl. Acad. Sci. USA 109, 4383–4388.

Rose, S., Marcellan, A., Hourdet, D., Creton, C., Narita, T., 2013. Dynamics of hybrid polyacrylamide hydrogels containing silica nanoparticles studied by dynamic light scattering. Macromolecules 46, 4567–4574.

Roy, N., Bruchmann, B., Lehn, J.-M., 2015. DYNAMERS: dynamic polymers as self-healing materials. Chem. Soc. Rev. 44, 3786–3807.

Rubinstein, M., Colby, R., 2003. Polymer Physics. Oxford University Press, Oxford.

Satarkar, N.S., Biswal, D., Hilt, J.Z., 2010. Hydrogel nanocomposites: a review of applications as remote controlled biomaterials. Soft Matter 6, 2364–2371.

Sijbesma, R.P., Beijer, F.H., Brunsveld, L., Folmer, B.J., Hirschberg, J.K., Lange, R.F., Lowe, J.K., Meijer, E., 1997. Reversible polymers formed from self-comple-mentary monomers using quadruple hydrogen bonding. Science 278, 1601–1604.

Skene, W.G., Lehn, J.-M.P., 2004. Dynamers: polyacylhydrazone reversible covalent polymers, component exchange, and constitutional diversity. Proc. Natl. Acad. Sci. USA 101, 8270–8275.

Sun, J.-Y., Zhao, X., Illeperuma, W.R., Chaudhuri, O., Oh, K.H., Mooney, D.J., Vlassak, J.J., Suo, Z., 2012. Highly stretchable and tough hydrogels. Nature 489, 133–136.

Sun, T.L., Kurokawa, T., Kuroda, S., Ihsan, A.B., Akasaki, T., Sato, K., Haque, M.A., Nakajima, T., Gong, J.P., 2013. Physical hydrogels composed of polyampholytes demonstrate high toughness and viscoelasticity. Nat. Mater. 12, 932–937.

Tee, B.C., Wang, C., Allen, R., Bao, Z., 2012. An electrically and mechanically self-healing composite with pressure-and flexion-sensitive properties for electronic skin applications. Nat. Nanotechnol. 7, 825–832.

Terryn, S., Brancart, J., Lefeber, D., Van Assche, G., Vanderborght, B., 2017. Self-healing soft pneumatic robots. Sci. Robot. 2, eaan4268.

Thakur, V.K., Kessler, M.R., 2015. Self-healing polymer nanocomposite materials: a review. Polymer 69, 369–383.

Toohey, K.S., Sottos, N.R., Lewis, J.A., Moore, J.S., White, S.R., 2007. Self-healing materials with microvascular networks. Nat. Mater. 6, 581–585.

Wang, C., Liu, N., Allen, R., Tok, J.B.H., Wu, Y., Zhang, F., Chen, Y., Bao, Z., 2013a. A rapid and efficient self-healing thermo-reversible elastomer crosslinked with graphene oxide. Adv. Mater. 25, 5785–5790.

Wang, C., Wu, H., Chen, Z., McDowell, M.T., Cui, Y., Bao, Z., 2013b. Self-healing chemistry enables the stable operation of silicon microparticle anodes for high-energy lithium-ion batteries. Nat. Chem. 5, 1042–1048.

Wang, Q., Gao, Z., 2016. A constitutive model of nanocomposite hydrogels with nanoparticle crosslinkers. J. Mech. Phys. Solids 94, 127–147.

Wang, Q., Gao, Z., Yu, K., 2017. Interfacial self-healing of nanocomposite hydrogels: theory and experiment. J. Mech. Phys. Solids 109, 288–306.

Wang, Q., Gossweiler, G.R., Craig, S.L., Zhao, X., 2015. Mechanics of mechanochemically responsive elastomers. J. Mech. Phys. Solids 82, 320–344.

Wang, Q., Mynar, J.L., Yoshida, M., Lee, E., Lee, M., Okuro, K., Kinbara, K., Aida, T., 2010. High-water-content mouldable hydrogels by mixing clay and a dendritic molecular binder. Nature 463, 339–343.

White, S.R., Sottos, N., Geubelle, P., Moore, J., Kessler, M.R., Sriram, S., Brown, E., Viswanathan, S., 2001. Autonomic healing of polymer composites. Nature 409, 794–797.

Whitlow, S.J., Wool, R.P., 1991. Diffusion of polymers at interfaces: a secondary ion mass spectroscopy study. Macromolecules 24, 5926–5938.

Wojtecki, R.J., Meador, M.A., Rowan, S.J., 2011. Using the dynamic bond to access macroscopically responsive structurally dynamic polymers. Nat. Mater. 10, 14–27.

Wool, R.P., 2008. Self-healing materials: a review. Soft Matter 4, 400–418.

Wu, D.Y., Meure, S., Solomon, D., 2008. Self-healing polymeric materials: a review of recent developments. Prog. Polym. Sci. 33, 479–522.

Wu, J., Zhao, Z., Hamel, C.M., Mu, X., Kuang, X., Guo, Z., Qi, H.J., 2018. Evolution of material properties during free radical photopolymerization. J. Mech. Phys. Solids 112, 25–49.

Xu, B., Li, H.J., Wang, Y.Y., Zhang, G.Z., Zhang, Q.S., 2013. Nanocomposite hydrogels with high strength crosslinked by titania. RSC Adv. 3, 7233–7236.

Yang, Y., Urban, M.W., 2013. Self-healing polymeric materials. Chem. Soc. Rev. 42, 7446–7467.

Yu, K., Wang, D., Wang, Q., 2018a. Tough and self-healable nanocomposite hydrogels for repeatable water treatment. Polymers 10, 880.

Yu, K., Xin, A., Wang, Q., 2018b. Mechanics of self-healing polymer networks crosslinked by dynamic bonds. J. Mech. Phys. Solids 121, 409–431.

Zhang, H., Wool, R.P., 1989. Concentration profile for a polymer-polymer interface. 1. Identical chemical composition and molecular weight. Macromolecules 22, 3018–3021.

Zhang, H., Zhao, Y., 2013. Polymers with dual light-triggered functions of shape memory and healing using gold nanoparticles. ACS Appl. Mater. Interfaces 5, 13069–13075.

Zhao, Z., Mu, X., Sowan, N., Pei, Y., Bowman, C.N., Qi, H.J., Fang, D., 2015. Effects of oxygen on light activation in covalent adaptable network polymers. Soft Matter 11, 6134–6144.

Zhao, Z., Mu, X., Wu, J., Qi, H.J., Fang, D., 2016. Effects of oxygen on interfacial strength of incremental forming of materials by photopolymerization. Extreme Mech. Lett. 9, 108–118.